European Polymer Journal 53 (2014) 90–99

Contents lists available at ScienceDirect

European Polymer Journal

journal homepage: www.elsevier.com/locate/europolj

Macromolecular Nanotechnolgy

Nanocomposites with superparamagnetic behavior based on a vegetable oil and magnetite nanoparticles

Cintia Meiorin [a], Diego Muraca [b], Kleber R. Pirota [b], Mirta I. Aranguren [a], Mirna A. Mosiewicki [a,*]

[a] Institute of Materials Science and Technology (INTEMA), University of Mar del Plata – National Research Council (CONICET), Av. Juan B. Justo 4302, 7600 Mar del Plata, Argentina
[b] Instituto de Física Gleb Wataghin (IFGW), Universidade Estadual de Campinas – UNICAMP, 6165 Campinas, São Paulo, Brazil

ARTICLE INFO

Article history:
Received 25 October 2013
Received in revised form 6 January 2014
Accepted 14 January 2014
Available online 27 January 2014

Keywords:
Vegetable oil
Nanocomposites
Magnetite nanoparticles
Magnetic properties
Shape memory properties

ABSTRACT

The direct reaction of unmodified tung oil and styrene initiated by boron trifluoride diethyl etherate allowed obtaining thermoset polymers with valuable properties like shape memory behavior. On the other hand, the addition of magnetite nanoparticles (MNPs) to the tung oil/styrene copolymer was considered, in order to improve/modify its properties. MNPs were synthesized by the method of alkaline coprecipitation, followed by coating with oleic acid in order to hydrophobize their surfaces and make them more compatible with the polymeric matrix. Thus, superparamagnetic polymer nanocomposites were prepared from the inclusion of the MNPs to the cationically copolymerized tung oil (TO) and styrene (St) networks. The morphology, dynamic–mechanical and mechanical properties of the copolymers as well as magnetic behavior were significantly affected by the variation of the concentration of the MNPs.

1. Introduction

During the last years, polymers from renewable resources have attracted an increasing attention, basically due to the low cost and large availability of the raw materials, as well as the potential biodegradability of their applications [1–4]. Consequently, increasing efforts have been devoted to the study of the synthesis conditions of polymeric precursors based on vegetable oils, their physicochemical characterization and determination of thermal and mechanical properties of the final materials [5–7].

Vegetable oils are the most widely used renewable resources due to their relatively low price, wide availability and potential reactivity through different chemical sites, their inherent biodegradability and low toxicity [8]. These oils are triglycerides composed of three fatty acids attached to a glycerol structure [6,9,10], which contain many reactive sites. In particular, tung oil is available as the major product from the seeds of the tung tree (Aleurites fordii) [11]. The principal constituent of this oil is a glyceride composed mainly of α-elaeostearic acid (77–82 wt.%) containing three conjugated double bounds, oleic acid (3.5–12.7 wt.%) with one double bond and linolenic acid (8–10 wt.%) with three nonconjugated double bonds [5,12,13]. This highly unsaturated, conjugated triene system makes it an excellent drying oil at room temperature, in presence of oxygen [12,14,15]. This characteristic makes it one of the most used oils, together with linseed oil, in the paint and varnish industry [16].

Additionally, shape memory polymers have the capability for changing their shapes from a temporary shape to a permanent shape upon application of an external thermal stimulus [17–20]. In the last years, shape memory polymers have become increasingly important because of their low cost, low density, high shape recoverability, and easy processibility compared to conventional shape memory alloys [21,22]. Copolymers obtained from tung oil and a

* Corresponding author. Tel.: +54 223 481 6600; fax: +54 223 481 0046.
E-mail address: mirna@fi.mdp.edu.ar (M.A. Mosiewicki).

http://dx.doi.org/10.1016/j.eurpolymj.2014.01.018
0014-3057/

reactive comonomer like styrene can exhibit these properties depending mainly on the polymerization conditions [23].

On the other hand, the use of small percentages of nanoparticles advantageously could change some polymer properties. Thus, depending on the nanoparticle characteristics, they can lead to an increase of the elastic modulus, glass transition temperature or electrical conductivity of a material without affecting other properties such as low density, impact resistance and shape memory properties [24,25], allowing new possible applications.

In the field of metal nanoparticles, ferrofluids are of great technological importance and represent a new class of materials consisting of magnetic nanoparticles dispersed as colloids, stabilized in a liquid carrier fluid and exhibiting magnetic properties like magnetorheology or superparamagnetism. The stability of these suspensions is achieved by coating the particles with surfactants consisting of long chain molecules, like oleic acid [26]. The alkaline precipitation method for magnetite was developed by Massart and Cabuil [27] and has been widely used by several authors to prepare micro and nanomagnetic particles with different coatings and functionalizations [28].

Magnetite particles (Fe_3O_4) incorporated into shape memory polymers could potentially induce a response of the material by the application of magnetic fields. This would allow using new triggering mechanisms to activate particular behaviors from these polymers. In particular, under an alternating magnetic field, these particles could produce heat, triggering the memory effects. This effect could be an alternative to more common activation procedures that involve physical contact between the polymer and the stimulus media, i.e. by non-contact magnetic activation.

Although recently has been published several works related with shape memory polymers and magnetic nanoparticles [29], the use of biobased polymer as a matrix in this type of materials is an unsolved scientific and technological problem with diverse potential applications and ecological benefits that have not yet reported.

The aim of this work is to synthesize magnetic nanoparticles to be incorporated in tung oil/styrene copolymers and to investigate the effect of this incorporation on the structural and magnetic properties of the nanocomposites obtained.

2. Experimental

2.1. Materials

The tung oil (TO) employed was a commercial product supplied by Cooperativa Agrícola Limitada de Picada Libertad, Argentina. Its composed mainly of α-elaeostearic acid (84 wt.%). Styrene (St) and tetrahydrofurane (THF) were purchased from Cicarelli laboratory, Argentina. Boron trifluoride diethyl etherate ($BF_3{\cdot}OEt_2$) with 46–51% BF_3 was obtained from Sigma–Aldrich and used as the initiator of the cationic reaction.

The following chemical products (Aldrich) were used as received in the synthesis of the magnetic nanoparticles: ferric chloride hexahydrate ($FeCl_3{\cdot}6H_2O$), ferrous chloride tetrahydrate ($FeCl_2{\cdot}4H_2O$), and ammonium hydroxide (28–30% NH_3). N-heptane was used as solvent (P.A. grade).

2.2. Methods and techniques

2.2.1. Magnetite nanoparticles (MNP) preparation

MNPs were prepared by a co-precipitation method from an aqueous Fe^{3+}/Fe^{2+} solution (molar ratio 3:2) using concentrated ammonium hydroxide in excess [27]. Specifically, 0.09 mol of $FeCl_3{\cdot}6H_2O$ and 0.06 mol of $FeCl_2{\cdot}4H_2O$ were dissolved in 50 mL of distilled water and heated at 70 °C. After that, 40 mL of NH_4OH were added and the formation of a black precipitated was immediately observed.

The particles were subsequently coated with oleic acid by adding 0.02 mol of the mentioned fatty acid and heating the suspension to 80 °C for 30 min [30]. The obtained oleic acid coated magnetite nanoparticles were washed with distilled water and separated by centrifugation several times until neutral pH was obtained. Finally, they were dispersed in n-heptane to form a stable ferrofluid and stored until further use.

2.2.2. Nanocomposites preparation

A tung oil/styrene weight ratio of 50/50 was the selected composition for the polymeric matrix (50TO/50St). The mixture was stirred and this step was followed by the addition of the modified initiator prepared by mixing tetrahydofuran, THF (5 wt.% with respect to the catalyst) with boron trifluoride diethyl etherate (3 wt.% with respect to the reactive mixture). Due to the poor miscibility of the catalyst in the oils, it must be modified to obtain a homogeneous initial solution [5,7,31]. A selected percent of oleic acid-coated magnetite (1 or 9 wt.%) was added to the original mixture. The chosen nomenclature was 50TO/50St-1MNP and 50TO/50St-9MNP, respectively. This mixture was put into an ultrasonic device to obtain a good dispersion of magnetite nanoparticles and finally, poured into glass plates of 13 mm × 18 mm separated by a rubber cord of 1 mm of thickness and kept closed with metal clamps. The reactants were heated first at 25 °C for 12 h, then at 60 °C for 12 h and finally at 100 °C for 24 h [23]. After curing, the samples were conditioned at room temperature, in a normally illuminated area, inside a desiccator containing silica gel to maintain a dry atmosphere.

2.2.3. Transmission electron microscopy (TEM)

Transmission electron microscopy (TEM) was used to determine the particle morphology, size and structure of the magnetite particles by JEOL 100 CX II (JAPAN, 1983) operating at 100 kV. The sample dispersions were drop-cast onto the copper grids separately.

2.2.4. X-ray diffraction (XRD)

X-ray diffraction (XRD) spectra of MNPs were obtained with a PANalytical X'Pert Pro diffractometer using a Cu Kα radiation source ($\lambda = 0.1546$ nm) operating at 40 kV and 40 mA.

2.2.5. Chemical characterization of the materials (FT-IR)

FTIR spectra of the magnetite particles with and without oleic acid were recorded by the attenuated total

reflection method (ATR) using a Thermo Scientific Nicolet 6700 FT-IR spectrometer. The spectra were recorded over the range of 500–4000 cm^{-1} with a resolution of 2 cm^{-1} and averaged over 32 scans.

2.2.6. Thermogravimetric analysis (TGA)

Thermogravimetric analysis of the magnetite particles with and without oleic acid and of the nanocomposites were performed using a TGA-50 SHIMADZU thermogravimetric analyzer at a heating speed of 10 °C/min under air atmosphere. The nanoparticles were previously dried in a vacuum oven until constant weight.

2.2.7. Dynamical–mechanical tests (DMA)

A Perkin Elmer dynamic mechanical analyzer (DMA 7) was used to determine the dynamic mechanical behavior of the films using the tensile fixture. The sample dimensions were 20 × 5 × 0.5 mm^3.

2.2.8. Mechanical tests

Microtensile testing: was performed at 18 °C on tensile specimens of 5 mm × 35 mm × 1 mm cut from the molded plaques, using a universal testing machine (INSTRON 8501), in accordance with ASTM D 1708-93 using a crosshead speed of 5 mm/min. Young's modulus (E), ultimate stress (σ_u) and elongation at break (ε_b) were determined from the average values of at least four replicates for each sample.

2.2.9. Static magnetic properties

The static magnetic properties were studied using a commercial SQUID magnetometer (Quantum Design, MPMS XL). In this way, both isothermal magnetization curves as well as ZFC/FC measurements were performed in order to characterize the static magnetic properties of the composites. The Zero field cooling/field cooling (ZFC/FC) measurement protocol was carried out as follows: the sample was first cooled down from 300 K to 5 K in zero magnetic field, then a static magnetic field of 50 Oe was applied and the magnetization was measured increasing the temperature up to 300 K. Subsequently the sample was cooled down to 5 K under the same applied magnetic field (50 Oe) and the magnetization was measured while warming up the sample from 5 K to 300 K.

2.3.0. Scanning electron microscopy (SEM)

Scanning electron microscopy (SEM) was used to obtain pictures of the fracture surfaces of composite materials using a scanning electron microscope Jeol JSM-6460LV equipped with detectors for secondary and reflected electrons. Samples were pre-coated with gold (sputtering).

3. Results and discussion

3.1. Synthesis and characterization of magnetite nanoparticles (MNP)

3.1.1. Transmission electron microscopy (TEM)

The magnetite particles coated with oleic acid show hydrophobic character that promote their stability in organic solvents and increases the compatibility with the polymeric matrix. Transmission electron microscopy allows obtaining information about the shapes and sizes of the particles. Fig. 1 shows the TEM images of the magnetite particles with and without oleic acid coating. While Fig. 1a denotes presence of agglomeration of the particles, Fig. 1b shows each particle separated from the neighbors because of the organic chain absorbed on its surface. Surfactant molecules (also called stabilizing agents) are attached to the nanoparticle surface, preventing clotting and providing the desired dispersion and surface properties. The size and shape of magnetite nanoparticles may vary depending on the nature and concentration of the stabilizing agent [32].

The statistics of the size distributions and average particle diameter were calculated from TEM images and are presented as histograms in Fig. 1. The nanoparticles without oleic acid have a size slightly higher than the oleic acid coated nanoparticles (average diameter: 11.1 nm and 9.8 nm, respectively). The reason for this may be that the calculation of the average diameter of the uncoated magnetite particles is affected by the size of aggregates that appear as single particles in the TEM images, resulting in a larger average size of the nanoparticles. Aggregation is clearly present as inferred from the histogram of uncoated particles, which is very asymmetrical with significant deviation towards large particle size (24–30 nm). This contribution is much less significant in the histogram corresponding to oleic acid coated magnetite.

3.1.2. X-ray diffraction (XRD)

The crystalline structure of the magnetite particles were determined by powder X-ray diffraction (XRD) as shown in Fig. 2. The positions and relative intensities of all diffraction peaks in Fig. 2 agree with those from the standard crystal of magnetite (Fe_3O_4) or maghemite (Fe_2O_3) [29,30,33,34].

The crystal size was determined using Scherrer's equation [35–37]:

$$D = \kappa \cdot \lambda / \beta \cdot \cos(\theta)$$

where κ = Scherrer constant (0.9) [38]; λ = radiation wavelength (Cu Kα = 0.1546 nm); β = width at half height of the selected peak in radians; θ = Bragg angle.

According to this equation, and using the diffraction signal corresponding to the (3 1 1) plane, the crystal size was calculated as 8.8 nm, close to the value obtained from TEM images. It is important to state that X-ray diffraction is sensitive to the crystallite size in the particles. However the "crystallite size" is not necessarily synonymous with "particle size" and this method is only an estimation of the diameter of the magnetite particles.

3.1.3. Chemical characterization (FT-IR)

Fig. 3 shows the comparison of the bare magnetite (A), oleic acid (B) and oleic acid coated magnetite (C) spectra. In curve A, the bands centered at 3340 cm^{-1} and 1630 cm^{-1} are assigned to O–H vibrations absorbed on the surface of Fe_3O_4 nanoparticles. The broad band of absorption in the range of 500–700 cm^{-1} corresponds to the Fe–O bonds of bulk magnetite. The curve corresponding to the oleic acid spectra (B) presents an intense peak at 1710 cm^{-1}

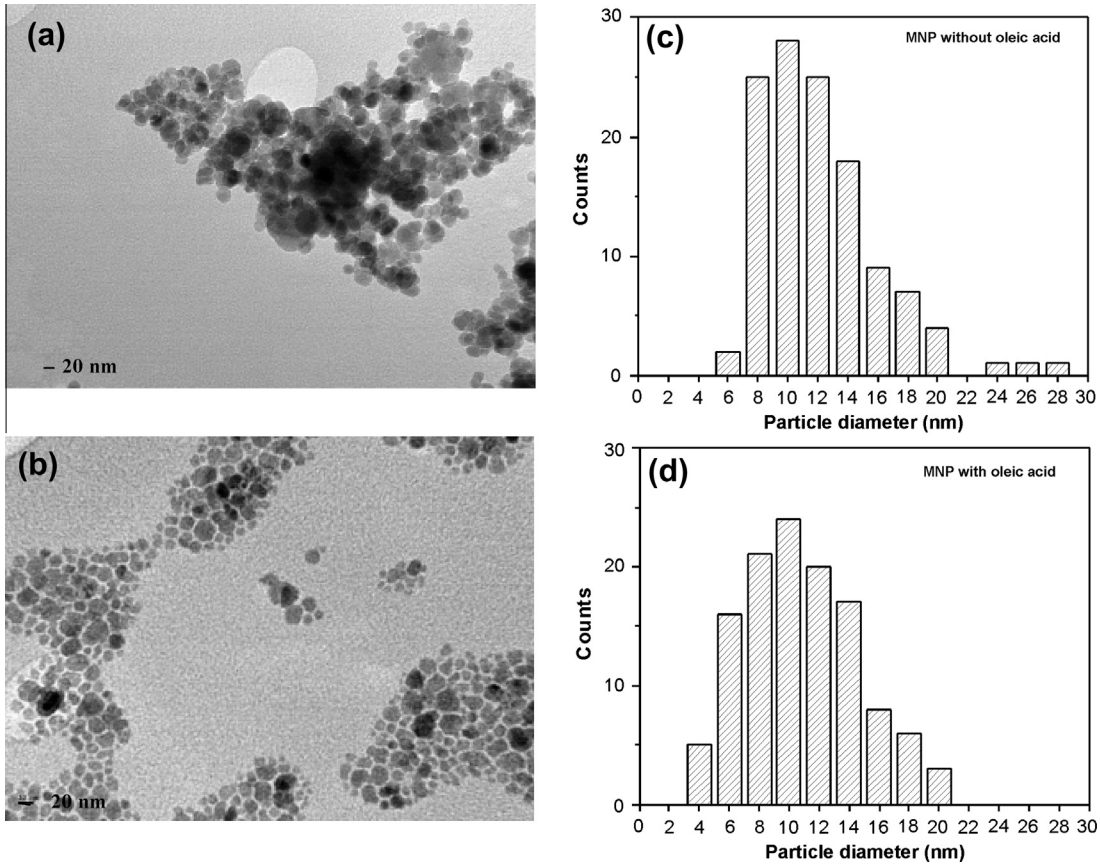

Fig. 1. TEM micrographs of the magnetite (a) and oleic acid coated magnetite (b) and the corresponding histograms (c and d).

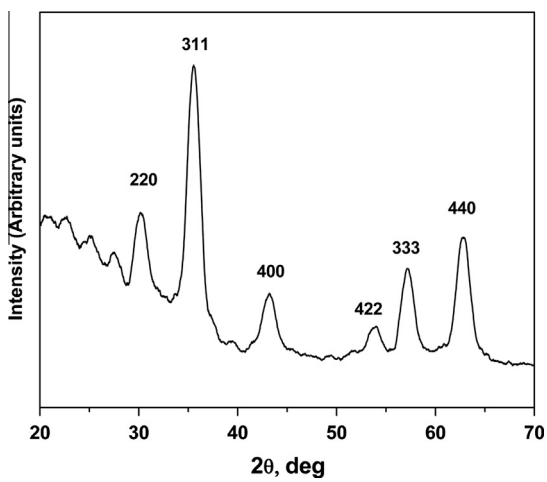

Fig. 2. XRD spectrum of magnetite MNPs.

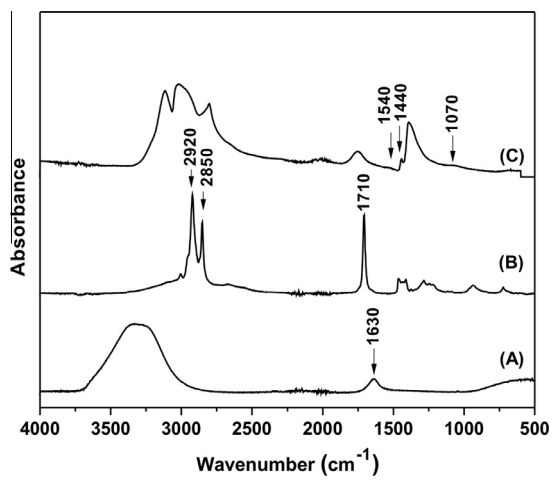

Fig. 3. FT-IR spectra of the bare magnetite (A), oleic acid (B) and oleic acid coated magnetite (C).

characteristic of the carbonyl stretch of the acid group. The two bands at 2920 and 2850 cm^{-1} can be attributed to asymmetric and symmetric stretching of C–H bonds respectively in methylene groups. The peak at 1710 cm^{-1} appears with low intensity in curve C. Additionally, a weak band at 1070 cm^{-1} appears, which is attributed to the C–O single bond stretch originated after adsorption of the oleic acid on the particles surface. The small shoulder at 1540 cm^{-1} could be caused by a covalent bond of the carboxylate with the structure of the magnetite [39,40]. The band at 1440 cm^{-1} can be ascribed to the coordinated

in-plane deformation of the hydroxyl groups of the carboxyl group of the oleic acid physiadsorbed on the particles surface [38]. These results revealed that oleic acid was physic and chemisorbed onto the Fe_3O_4 nanoparticles as a carboxylate [41,42].

3.1.4. Thermogravimetric analysis (TGA)

The oleic acid amount on the surface of the magnetite nanoparticles was determined by thermogravimetric analysis in air atmosphere (Fig. 4). Although the nanoparticles were previously dried in a vacuum oven to constant weight, the curve of weight loss versus temperature for magnetite shows a small initial mass loss around 100 °C attributed to water evaporation due to the high hydrophilicity of the samples. The thermal degradation curve of magnetite coated with oleic acid shows no significant initial water loss and the most important degradation step is observed in the temperature range 150–400 °C related with the decomposition of the organic surfactant. The relative amount of oleic acid on magnetite was determined as 19.5%, calculated from the residual mass after degradation of the organic coating. Mass gain observed in both samples curves at higher temperatures is related to the thermal degradation in air atmosphere that produces the oxidation reaction of magnetite (Fe_3O_4) to iron oxide (III), Fe_2O_3. That is, for the same amount of Fe originally present, the amount of oxygen is increased due to the reaction and this is reflected in an increase in mass.

3.2. Characterization of nanocomposites

3.2.1. Thermogravimetric analysis (TGA)

Thermogravimetric tests were conducted on neat TO/St copolymers and on the nanocomposites to evaluate the effect of the addition of nanoparticles on the thermal degradation of the materials.

Fig. 5 shows thermogravimetric curves (TGA) for the sample of 50TO/50St with 0, 1 and 9 wt.% of magnetite nanoparticles in air atmosphere. Residual mass at 800 °C allowed confirming the relatively high percentage of nanoparticles contained in the sample 50TO/50St-9MNP. The curves with 1 and 9 wt.% of MNP show a greater weight loss between 150 and 400 °C than the matrix without nanoparticles due thermal degradation of oleic acid that covers the magnetite particles surface.

Hence, the presence of nanoparticles alters the polymer structure, which leads to changes in the degradation mechanisms.

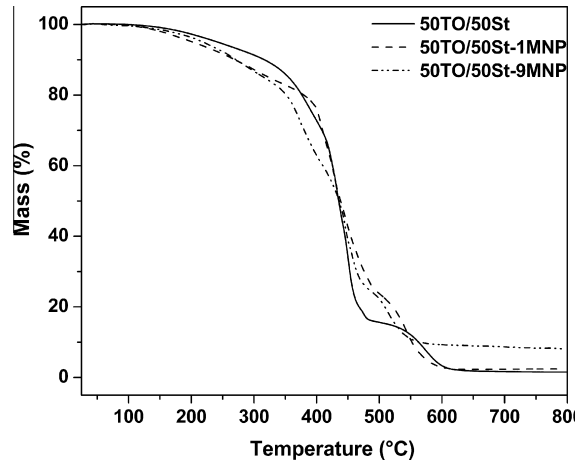

Fig. 5. Thermogravimetric curves for sample 50TO/50St with 0, 1 and 9 wt.% of MNP.

3.2.2. Dynamical-mechanical tests (DMA)

Fig. 6a shows the variation in tan δ as a function of temperature for 50TO/50St copolymers with and without addition of MNP.

For the sample with 1 wt.% of MNP it could be observed that the maximum on tan δ curve shifts to higher temperatures due to the addition of MNP, while the shape of the curve also suffers an important change, since two peaks can be observed for the nanocomposite. One of them matches with the glass transition temperature of the

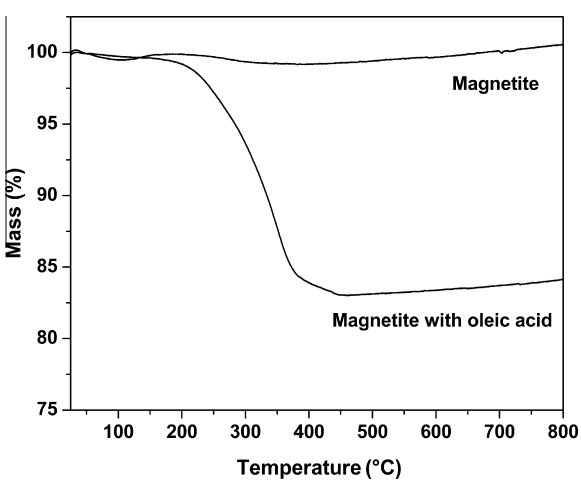

Fig. 4. Thermogravimetric curves for magnetite nanoparticles with and without oleic acid.

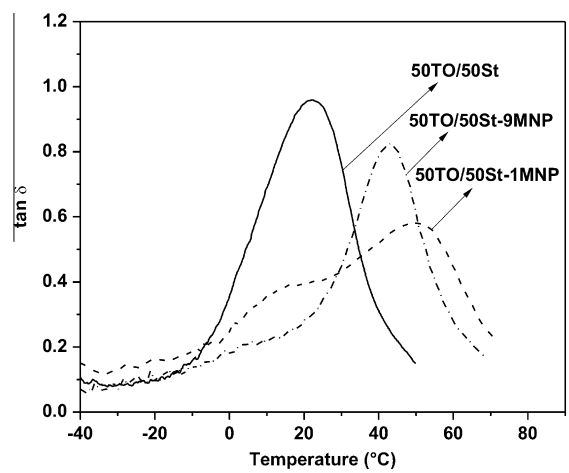

Fig. 6a. tan δ vs temperature curves for the 50TO/50St copolymer with 0, 1 and 9 wt.% of MNP.

matrix (around 20 °C) while the second one presents its maximum at 50.3 °C. This can be attributed to the heterogeneity of the system, some regions in the sample correspond to the bulk polymer, essentially unaffected by the incorporation of the MNP, and some regions are affected by interactions with the nanoparticles. For example, the oleic acid chains that constitute the coating of the nanoparticles can interact through Van der Waal forces with the fatty acid chains in the matrix. Additionally, the carbon–carbon insaturation of the oleic acid can also participate in the cationic copolymerization of the matrix and in this way become part of the network through the formation of interfacial covalent bonds. With the addition of MNP different relaxation mechanisms and inhomogeneities appears in the material. For the copolymer having 9 wt.% MNP only a peak is observed at 43 °C, since most of the material is affected by the presence of a relatively large concentration of nanoparticles.

The comparison of the 50TO/50St curves with the addition of 0, 1 and 9 wt.% of MNP also shows that the peak height is lower for samples with MNP and that the transition is broader. This result is related to a more heterogeneous network as mentioned previously. All copolymers with MNP addition maintained good damping properties, similarly to those presented by the unfilled polymer [23] with maximum intensity of the loss factor above 0.3 in a broad range around room temperature. This condition is sought for applications requiring high energy absorption [43].

The storage modulus (Fig. 6b) increases with the MNP incorporation with respect to the unfilled polymer throughout the temperature range studied. There are minor differences between the curves corresponding to the nanocomposites.

3.2.3. Mechanical Tests and shape memory properties

A summary of the mechanical properties measured from tensile tests is presented in Table 1. It can be observed that addition of MNP to the 50TO/50St copolymers

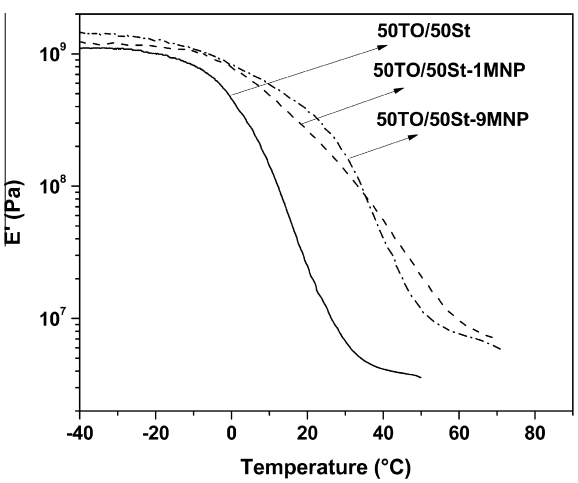

Fig. 6b. Storage modulus as a function of the temperature for the 50TO/50St copolymer with 0, 1 and 9 wt.% of MNP.

Table 1
Tensile properties of 50TO/50St copolymers with 0 and 1 wt.% of MNP.

Sample	E (MPa)	σ_u (MPa)	ε_u (%)
50TO/50St	3.30 ± 0.36	1.36 ± 0.41	45.88 ± 10.89
50TO/50St-1MNP	3.98 ± 0.93	1.08 ± 0.43	35.58 ± 14.11

allowed to increase the Young's modulus of the new materials. For samples with 50TO/50St is observed that the addition of 1 wt.% of MNP produced no significant change in resistance, but the ultimate strain decreases as a result of new fracture mechanisms involved. The presence of nanoparticles stiffens the material, fragility increases and the ultimate strain decreases.

The shape memory behavior of these novel nanocomposites was investigated. A sample with the initial shape of a rectangular bar (permanent shape) was deformed into a secondary transient form of "*U*" at a temperature of 70 °C, that is a temperature above the Tg of the material, which behaves as a rubber under this condition. After cooling and releasing the applied load, the "*U*" temporary shape remains fixed (Fig. 7a). The recovery process occurs when the material is heated again in water at a temperature of 70 °C allowing the material to recover its original rectangular shape (Fig. 7f). Under the mentioned condition the samples the samples 50TO/50St with 1 wt.% of MNP presented shape memory properties, a response that is governed exclusively by the polymer matrix. Fig. 7 shows the photos of the tests performed for copolymers of 50TO/50St with 1 wt.% of MNP, where the recovery time was approximately 5 s.

3.2.4. Magnetic properties

Fig. 8 shows the temperature dependence of the magnetization taken in the ZFC and FC processes (in the temperature range 5–300 K) measured at 50 Oe for the sample of 50TO/50St with 1 wt.% of MNP. The typical behavior associated with arrangements of superparamagnetic nanoparticles can be observed with a maximum in the curve of ZFC that indicates the change from the superparamagnetic state to the blocked state [44,45]. From the ZFC, the mean blocking temperature (defined as the maximum of d(FC–ZFC)/dT) and the blocking temperature, T_{Bmax} (defined as the maximum in the curve of ZFC) were determined (16 K and 70 K, respectively). From the shape of d(FC–ZFC)dT (narrow blocking temperature distribution) and the small difference between the maximum on the ZFC curve temperature and the irreversibility temperature (defined as the threshold temperature above which FC and ZFC curves coincide), a very narrow distribution in size of these nanoparticles can be inferred, as well as absence of particle–particle agglomeration and inter-particle interactions.

Fig. 9 shows the magnetization curves as a function of the applied field at different temperatures (10, 70 and 300 K), for the copolymer of 50TO/50St with 1 wt.% of MNP. A magnification of the central area of the magnetization loops at these temperatures are shown in the inset of Fig. 9 in order to have a better description of the coercive fields behavior. From this, the superparamagnetic behavior

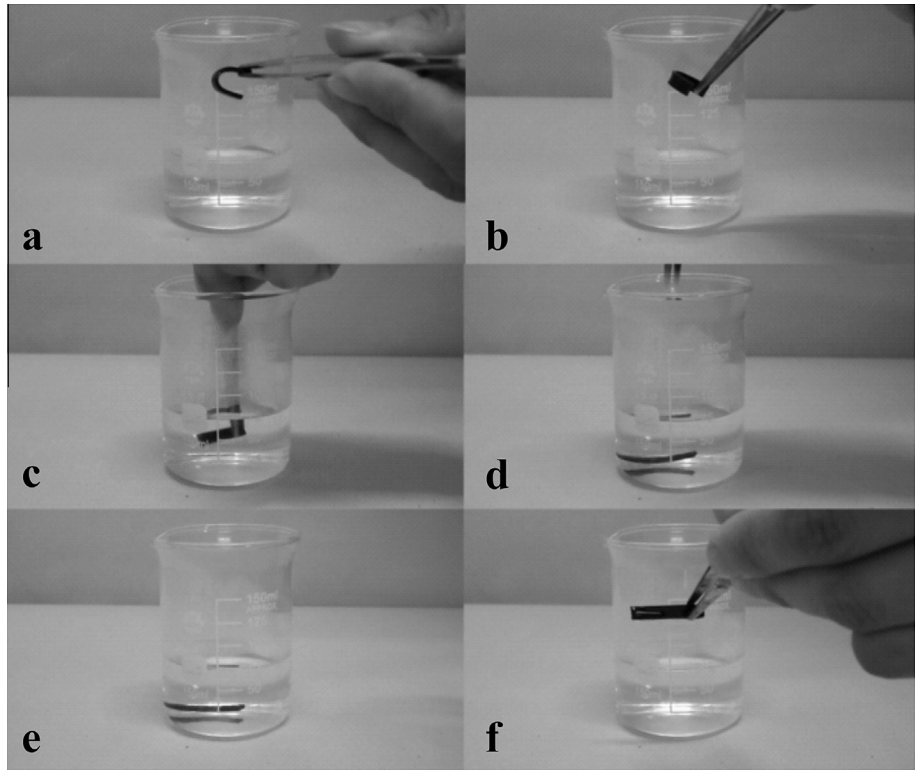

Fig. 7. Shape memory behavior for the copolymer of 50TO/50St-1MNP.

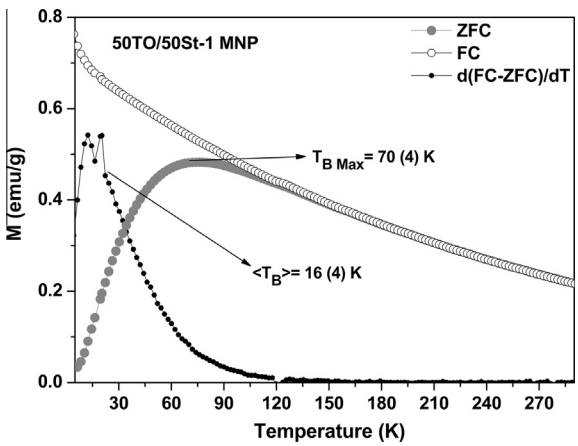

Fig. 8. Magnetization versus temperature for the copolymer of 50TO/50St with 1 wt.% of MNP, measured at 50 Oe under zero field cooling, ZFC (solid circles) and field cooling, FC (open circles) conditions.

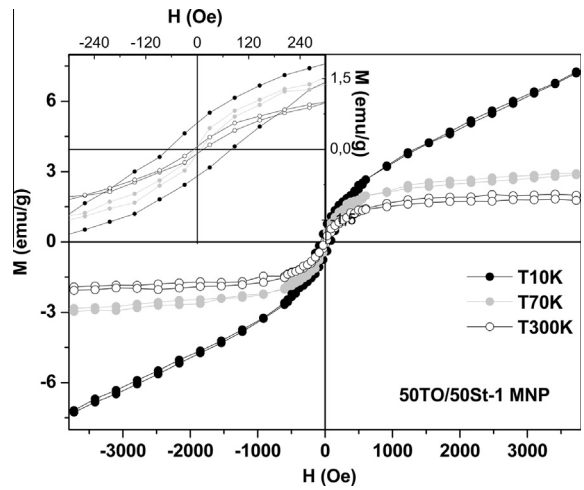

Fig. 9. Magnetization curves for the copolymer of 50TO/50St with 1 wt.% of MNP at different temperatures.

of the nanocomposites above a temperature of 70 K can be confirmed. For temperatures below T_B, the magnetic particles are blocked, and the magnetic moment is fixed (magnetic relaxation time at that temperature is greater than the measurement time) and consequently, hysteresis appears in the magnetization curve. A small and depreciable value of coercive field (less than 10 Oe) can be observed from the hysteresis loop at room temperature. This could be due to a small dipolar interaction between some of the nanoparticles in the copolymer. Hence the magnetic properties of the material are determined by the superparamgnetic properties of an ensemble of individual nanoparticles without interaction and not due to a collective behavior.

Fig. 10 shows the dependence of the magnetization as a function of temperature in the ZFC and FC processes for the sample of 50TO/50St with 9 wt.% of MNP. As observed for the sample with 1 wt.% of MNP, this sample also presents a behavior associated to the arrangement of particles

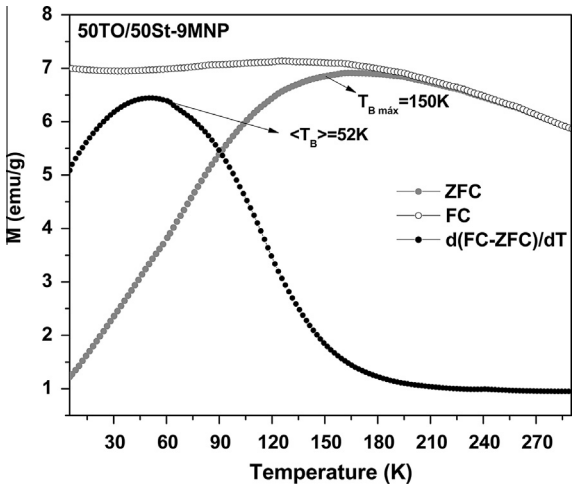

Fig. 10. Magnetization versus temperature for the copolymer of 50TO/50ST with 9 wt.% of MNP, measured at 50 Oe under zero field cooling, ZFC (solid circles) and field cooling, FC (open circles) conditions.

Table 2
Magnetic properties for the nanocomposites with 1 and 9 wt.% of MNP.

Sample	T_{Bmax} (K)	$\langle T_B \rangle$ (K)	$T_{irreversibility}$(K)
50TO/50St-1MNP	70	16	92
50TO/50St-9MNP	150	52	165

affected by the presence of dipolar interaction between the magnetic nanoparticles. In this case, the values of the average blocking temperature and the maximum blocking temperature are 52 K and 150 K, respectively.

Comparing the curves ZFC/FC of the samples with different contents of MNP it could be seen that the sample containing 1 wt.% MNP (Fig. 9, Table 2) exhibits different magnetic properties with respect to the sample having with 9 wt.% of MNP (Fig. 10, Table 2). As it was expected, the blocking temperature increases with the concentration of MNP, which is associated with the increase in dipolar interactions between nearby nanoparticles. Moreover, the maximum in the ZFC curve is wider, which is possibly associated with interactions between particles. Finally, the low temperature saturation becomes evident in FC curves for the sample with 9 wt.% of MNP while the magnetization continues to increase with decreasing temperature for the material with 1 wt.% of MNP; that indicates that dipolar interactions are stronger in the nanocomposite with more particles. Consequently, the presence of aggregates, the local concentration and dipolar interactions between particles determine the collective magnetic behavior of the particles in this sample [29].

3.2.5. Study of the morphology of the copolymers of 50TO/50St with 1 and 9 wt.% of MNP

Fig. 11 shows brittle fracture surfaces obtained after immersion in liquid nitrogen with a magnification of 50×

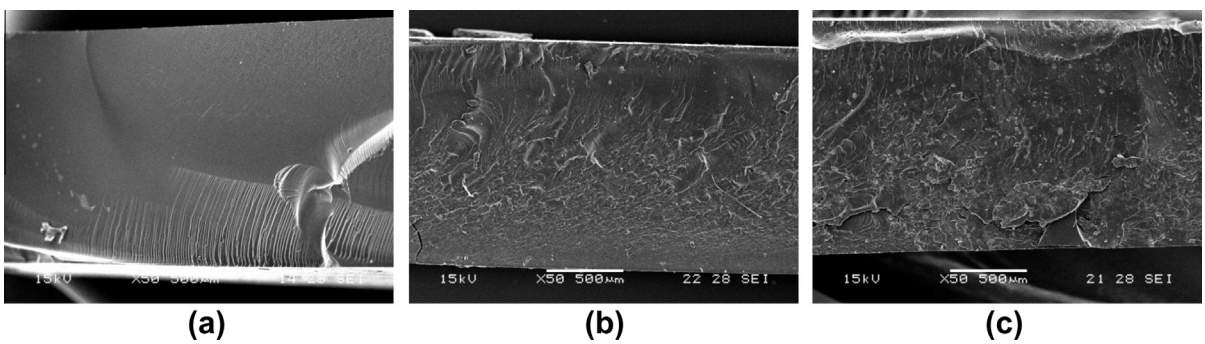

Fig. 11. SEM morphologies for the copolymers of 50TO/50St (a) with 1 and 9 wt.% of MNP (b and c).

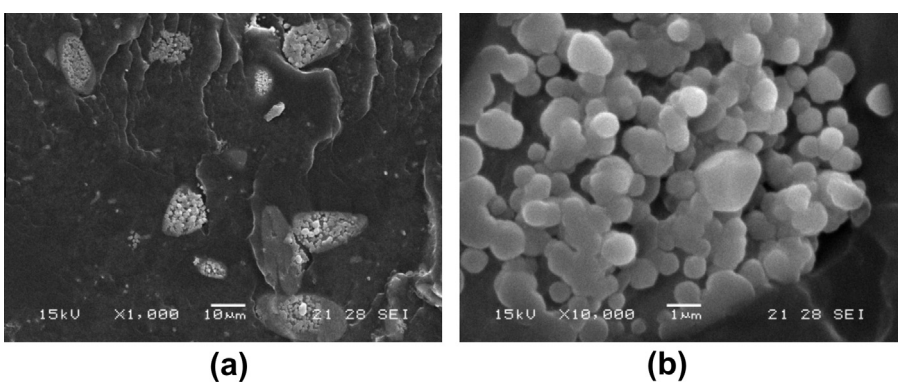

Fig. 12. SEM morphologies for the copolymers of 50TO/50St with 9 wt.% of MNP (1000× (a) and 10000× (b)).

for the copolymers of 50TO/50St (Fig. 12a) with 1 and 9 wt.% of MNP (Fig. 11b and c).

Fig. 11a shows the fracture surface of the unreinforced matrix, which shows no signs of plastic deformation. This smooth surface is typical of brittle fracture in unmodified resins. The presence of nanoparticles in the copolymer generates the occurrence of different mechanisms of fracture propagation and consequently, differences in the obtained SEM micrographs. The surface roughness increases markedly with the incorporation of MNP which indicates an increase in energy dissipation during fracture.

The presence of rigid nanoparticles arrest and change the crack progress in the material. This change in texture has been previously observed by several authors in different types of polymers [46–50].

Fig. 12 shows the images with higher magnification of the sample of 50TO/50St with 9 wt.% of MNP (1000×, (13.a) and 10,000× (13.b)). The images confirm the presence of particle agglomeration. The particle size observed is about 10 nm, as was mentioned in the MNP characterization.

4. Conclusions

Magnetite nanoparticles, MNP, were successfully synthesized and coated with oleic acid to obtain stable suspensions in heptane.

The nanocomposites obtained by adding MNP to the tung oil-based copolymers synthesized showed superparamagnetic behavior.

The morphology of the novel nanocomposites observed in fracture surfaces showed an increase in the surface roughness with the incorporation of MNP, which indicates an increase in energy dissipation during fracture.

The dynamic mechanical properties were appreciably affected by the incorporation of MNP, as a consequence of the different relaxation mechanisms and inhomogeneities that appeared in the material because of the presence of the nanoparticles.

Additionally, the incorporation of MNP stiffens the material and reduces the ultimate strain, also increasing its fragility. The shape memory properties of the matrix is also observed in the nanocomposites.

Comparison of the magnetic properties of the nanocomposites allowed to identify a transition from superparamagnetic (low concentration) to interaction superparamagnetic (high concentration) regime. From these observation, it was concluded that to preserve the superparamagnetic regime on high concentration of MNPs is necessary to improve the level of particle dispersion in the reactive mixture.

Acknowledgements

The authors thank the Cooperativa Agrícola de Picada Libertad for samples of tung oil, the financial support of CONICET, UNMdP and ANPCyT from Argentine; and FAPESP and UNICAMP from Brazil.

References

[1] Yu L, Dean K, Li L. Polymer blends and composites from renewable resources. Prog Polym Sci 2006;31(6):576–602.
[2] Kaplan DL. Biopolymers from renewable resources. New York: Springer; 1998.
[3] Mohanty AK, Misra M, Drzal LT. Natural fibers, biopolymers, and biocomposites. Boca Raton, Florida: Taylor & Francis; 2005.
[4] Mecking S. Nature or petrochemistry?–biologically degradable materials. Angew Chem Int Ed Engl 2004;43(9):1078–85.
[5] Li F, Larock RC. Thermosetting polymers from cationic copolymerization of tung oil: synthesis and characterization. J Appl Polym Sci 2000;78(5):1044–56.
[6] Khot SN, Lascala JJ, Can E, Morye SS, Williams GI, Palmese GR, et al. Development and application of triglyceride-based polymers and composites. J Appl Polym Sci 2001;82(3):703–23.
[7] Li F, Larock RC. New soybean oil–styrene–divinylbenzene thermosetting copolymers. I. Synthesis and characterization. J Appl Polym Sci 2001;80(4):658–70.
[8] Lu Y, Larock RC. Novel polymeric materials from vegetable oils and vinyl monomers: preparation, properties, and applications. ChemSusChem 2009;2(2):136–47.
[9] Lu Y, Larock RC. Bio-based nanocomposites from corn oil and functionalized organoclay prepared by cationic polymerization. Macromol Mater Eng 2007;292(7):863–72.
[10] Petrović ZS, Zhang W, Javni I. Structure and properties of polyurethanes prepared from triglyceride polyols by ozonolysis. Biomacromolecules 2005;6(2):713–9.
[11] Wood EC. Tung oil: a new American industry, 1949.
[12] Liu C, Yang X, Cui J, Zhou Y, Hu L, Zhang M, et al. Tung oil based monomer for thermosetting polymers: synthesis, characterization and copolymerization with styrene. BioResources 2012;7(1):447–63.
[13] Mosiewicki MA, Casado U, Marcovich NE, Aranguren MI. Polyurethanes from tung oil: polymer characterization and composites. Polym Eng Sci 2009;49(4):685–92.
[14] Kinabrew RG. Tung oil in Mississippi, the competitive position of the industry. MS: University of Mississippi; 1952.
[15] Li F, Larock RC. Synthesis, structure and properties of new tung oil – styrene – divinylbenzene copolymers prepared by thermal polymerization. Biomacromolecules 2003;4(4):1018–25.
[16] Gandini A. Monomers and macromonomers from renewable resources. Biocatalysis in Polymer Chemistry: Wiley-VCH; 2010. p. 1–33.
[17] Biju R, Gouri C, Reghunadhan Nair CP. Shape memory polymers based on cyanate ester-epoxy-poly (tetramethyleneoxide) co-reacted system. Eur Polym J 2012;48(3):499–511.
[18] Lendlein A. Shape-memory polymers. New York: Springer; 2010.
[19] Hu J, Zhu Y, Huang H, Lu J. Recent advances in shape-memory polymers: structure, mechanism, functionality, modeling and applications. Prog Polym Sci 2012;37:1720–63.
[20] Mather PT, Luo X, Rousseau IA. Shape memory polymer research. Annu Rev Mater Res 2009:445–71.
[21] Li F, Larock RC. New soybean oil–styrene–divinylbenzene thermosetting copolymers. V. shape memory effect. J Appl Polym Sci 2002;84:1533–43.
[22] Wei ZG, Sandström R, Miyazaki S. Shape-memory materials and hybrid composites for smart systems – Part I shape-memory materials. J Mater Sci 1998;33(15):3743–62.
[23] Meiorin C, Aranguren MI, Mosiewicki MA. Vegetable oil/styrene thermoset copolymers with shape memory behavior and damping capacity. Polym Int 2012;61(5):735–42.
[24] Parulekar Y, Mohanty AK. Biodegradable toughened polymers from renewable resources: blends of polyhydroxybutyrate with epoxidized natural rubber and maleated polybutadiene. Green Chem 2006;8(2):206–13.
[25] Thulasiraman V, Rakesh S, Sarojadevi M. Synthesis and characterization of chlorinated soy oil based epoxy resin/glass fiber composites. Polym Compos 2009;30(1):49–58.
[26] Iannone A, Magin RL, Walczak T, Federico M, Swartz HM, Tomasi A, et al. Blood clearance of dextran magnetite particles determined by a noninvasive in vivo ESR method. Magnet Reson Med 1991;22(2):435–42.
[27] Massart R, Cabuil V. Synthèse en milieu alcalin de magnétite colloïdale: contrôle du rendement et de la taille des particules = synthesis of colloidal magnetite in alkaline medium: yield and particle size control. J Chim Phys 1987;84(7–8):967–73.
[28] Yang J, Park SB, Yoon HG, Huh YM, Haam S. Preparation of poly ε-caprolactone nanoparticles containing magnetite for magnetic drug carrier. Int J Pharm 2006;324:185–90.

[29] Puig J, Hoppe CE, Fasce LA, Pérez CJ, Piñeiro-Redondo Y, Bañobre-López M, et al. Superparamagnetic nanocomposites based on the dispersion of oleic acid-stabilized magnetite nanoparticles in a diglycidylether of bisphenol a-based epoxy matrix: magnetic hyperthermia and shape memory. J Phys Chem C 2012;116(24):13421–8.
[30] Yeganeh H, Hojati-Talemi P. Preparation and properties of novel biodegradable polyurethane networks based on castor oil and poly(ethylene glycol). Polym Degrad Stab 2007;92(3):480–9.
[31] Li F, Marks DW, Larock RC, Otaigbe JU. Fish oil thermosetting polymers: synthesis, structure, properties and their relationships. Polymer 2000;41:7925–39.
[32] Mosivand S, Monzon L, Kazeminezhad I, Coey J. Influence of growth conditions on magnetite nanoparticles electro-crystallized in the presence of organic molecules. Int J Mol Sci 2013;14(5):10383–96.
[33] Ling Z, Rong H, Hong-Chen G. Oleic acid coating on the monodisperse magnetite nanoparticles. Appl Surf Sci 2006;253:2611–7.
[34] Schmid G. Nanoparticles: from theory to application. second ed. Verlag: Weinheim: Wiley; 2005.
[35] Scherrer P. Göttinger nachrichten gesell. J Math Phys 1918;2(26):98.
[36] Klug HP, Alexander LE. X-ray diffraction procedures: for polycrystalline and amorphous materials. second ed. New York: John Wiley & Sons Inc.; 1974.
[37] Patterson AL. The Scherrer formula for X-ray particle size determination. Phys Rev 1939;56(10):978–82.
[38] González M, Martín-Fabiani I, Baselga J, Pozuelo J. Magnetic nanocomposites based on hydrogenated epoxy resin. Mater Chem Phys 2012;132(2–3):618–24.
[39] Wang CY, Hong JM, Chen G, Zhang Y, Gu N. Facile method to synthesize oleic acid-capped magnetite nanoparticles. Chin Chem Lett 2010;21(2):179–82.
[40] Maity D, Choo SG, Yi J, Ding J, Xue JM. Synthesis of magnetite nanoparticles via a solvent-free thermal decomposition route. J Magn Magn Mater 2009;321(9):1256–9.
[41] Zhang L, He R, Gu H-C. Oleic acid coating on the monodisperse magnetite nanoparticles. Appl Surf Sci 2006;253:2611–7.
[42] Machunsky S, Grimm P, Schmid HJ, Peuker UA. Liquid–liquid phase transfer of magnetite nanoparticles. Colloids Surf, A 2009;348(1–3):186–90.
[43] Rao MD. Recent applications of viscoelastic damping for noise control in automobiles and commercial airplanes. J Sound Vibration 2003;262(3):457–74.
[44] Rajan GS, Stromeyer SL, Mauritz KA, Miao G, Mani P, Shamsuzzoha M, et al. Superparamagnetic nanocomposites based on poly(styrene-b-ethylene/butylene-b-styrene)/cobalt ferrite compositions. J Magn Magn Mater 2006;299(1):211–8.
[45] Ennas G, Casula MF, Falqui A, Gatteschi D, Marongiu G, Marras S, et al. Non-stoichiometric $CoFe_2O_4$ nanoparticles supported on an amorphous silica matrix. J Sol–Gel Sci Technol 2003;26(1–3):463–6.
[46] Cantwell WJ, Roulin-Moloney AC. In fractography and failure mechanisms of polymers and composites. In: Roulin-Moloney AC, editor. London, UK: Elsevier Applied Science; 1989. p. 256–8 [cap. 7].
[47] Cantwell WJ, Roulin-Moloney AC, Kaiser T. Fractography of unfilled and particulate-filled epoxy resins. J Mater Sci 1988;23(5):1615–31.
[48] Bandyopadhyay S. Review of the microscopic and macroscopic aspects of fracture of unmodified epoxy resins. Mater Sci Eng, A 1990;125(2):157–84.
[49] Kausch HH. Polymer fracture. 2nd ed. Germany: Springer Verlag; 1987. p. 382 [chap. 9].
[50] Marcovich NE, Auad ML, Bellesi NE, Nutt SR, Aranguren MI. Cellulose micro/nanocrystals reinforced polyurethane. J Mater Res 2006;21(4):870–81.